

Received 22 November 2023, accepted 9 December 2023, date of publication 18 December 2023,
date of current version 26 December 2023.

Digital Object Identifier 10.1109/ACCESS.2023.3344465

RESEARCH ARTICLE

A Coarse-to-Fine Approach for Rectifying Distorted Latent Fingerprints From Crime Scenes

QING BAO^{1,2}, YA-GANG WANG¹, CHANG GAO², LIANGXIAO SHA²,
AND FEIFEI LEE¹, (Member, IEEE)

¹Institute of Intelligent Rehabilitation Engineering, University of Shanghai for Science and Technology, Shanghai 200093, China

²Shanghai Key Laboratory of Scene Evidence, Shanghai 200083, China

Corresponding author: Feifei Lee (feifeilee@ieee.org)

This work was supported by the Shanghai Key Laboratory of Scene Evidence under Grant 2023XCWZK02.

ABSTRACT With the widely used fingerprints to identify criminals, the influence of fingerprint deformation arouses attention in forensic science. To date, many approaches have been proposed to rectify distorted fingerprints. However, the performance in handling low-quality fingerprints extracted at a crime scene is less high quality than expected. This paper presents a combined method to rectify the latent fingerprints extracted at a crime scene. The method is a coarse-to-fine approach, combining the robustness of traditional pattern recognition and the accuracy of deep learning networks. We conducted several experiments to compare our approach with other approaches, including the nearest-neighbor search and network methods. The results show a remarkable improvement in fingerprint matching, especially in low-quality latent fingerprints. The top 25 cumulative match rate improves from 0.65 (original) to 1 (proposed method), whereas other approaches improve the result to 0.85 at best.

INDEX TERMS Latent fingerprints, distortion rectification, coarse-to-fine method, DCNN.


I. INTRODUCTION

Fingerprints refer to the impression left by the ridges on the human finger. The primary reason for the widespread adoption of the automated fingerprint identification system (AFIS) is that the error rates are extremely low on high-quality fingerprint images [1]. AFIS is typically used in security domains. There are two primary recognition scenarios. In the positive scenario, the system should identify the user; in the negative scenario, the user's interest (e.g., criminal) is unwilling to be identified. These systems use an automated procedure to identify a person based on captured images stored in the system [2]. However, the recognition rate for low-quality fingerprints is far from satisfactory, and low-quality images are not uncommon [3], [4].

Fingerprints are one of the most crucial biometric identifications in forensic science for their uniqueness and stability. In the past several decades, AFIS has assisted in many criminal investigations. The typical AFIS comprises three primary steps. First, a raw fingerprint image is read with

preprocessing. Second, the ridge patterns, local features, and minutiae are extracted. Third, a matching score between two fingerprints is calculated by pairing the features extracted in the second step. The core of AFIS involves determining the similarity degree between fingerprints by the ridge structure and the distribution of minutiae points [5]. The distortion in fingerprint images primarily significantly reduces the matching score. Therefore, the fingerprint matcher is sensitive to image quality [6]. Distortion rectification transforms the distorted fingerprint into a normal one to increase the matching score [7].

Since fingerprints are the oldest biometric traits, many techniques and algorithms have been proposed in the literature for fingerprint recognition [8]. Studies on removing fingerprint distortion in forensics have considerably improved in recent years [9]. The most widely used distorted correction algorithms are minutiae-based methods [10]. Minutiae are discriminating and dependable. The primary idea of minutiae-based methods is to search for optimal matched minutiae pairs between distorted and reference fingerprints [11], [12], [13], [14]. Based on minutiae-matching methods, ridge-based methods have been presented

The associate editor coordinating the review of this manuscript and approving it for publication was Daniel Augusto Ribeiro Chaves .

to improve the accuracy. Similarly, these algorithms aim to find optimal ridges matching [15], [16], [17], [18]. Multiple attractive feature-extracting algorithms have been proposed to correct distorted fingerprints [13], [19], [20], [21], [22], [23]. These new algorithms are much more accurate than traditional minutiae-based or ridge-based methods. With the development of convolutional neural networks (CNNs), some scholars have proposed approaches based on convolutional network techniques [24], [25], [26], [27], improving accuracy with fewer constraints. Despite deep convolutional neural networks demonstrate its extraordinary power on various tasks. However, it is still changing to deploy state-of-art models into real-work applications [28]. In forensics, the search result of low-quality distorted fingerprints in large-capacity databases is far from satisfactory.

Some literature proved validity in the public test databases, including FVC2004 DB1, FVC2006 DB2, Tsinghua DF, NIST SD14, and NIST SD27 [13], [19], [20], [21], [22], [23], [24], [25], [26], [27], [29]. Application scenarios are limited in practical work due to two primary reasons. (1) The capacity of the test database is too small. The typically used largest database is NIST SD14, containing 27,000 fingerprints. Improving tens of thousands of databases does not make much sense in forensic science because we focus on rank improvement rather than the score. Experts would check the watch list given by AFIS. If there is a genuine match in the top 50 candidates, we regard the result as a hit; otherwise, it is a missed result. In practice, the low-quality latent fingerprints extracted in crime scene investigations (CSIs) can obtain a missed result when searching a database containing tens of millions of fingerprints. (2) The fingerprints in the test database differ considerably from those extracted in CSIs. Ridges overlapping, interrupting, and blurring, interference of the object background, the uneven surface of the object, surface attachment, and interference after enhancing latent fingerprints are typical factors reducing fingerprint quality.

In the convolution process, the input fingerprint image would be divided into many small blocks to extract features. Most samples in the test database selected to evaluate the performance in published literature are inked images. The orientation and ridges maps could be calculated reliably due to coherent and high-contrast ridges with little interference. Latent fingerprints with various interferences mentioned above are common in CSI, for the clear traces are more likely to be cleaned up by criminals to avoid investigation. Distorted fingerprints extracted on curved objects are usually challenging to identify for AIDS. Serious nonlinear distortion would reduce the performance of minutiae-based methods, and the interferences caused by attachment, ridges, background, the surface of an object, and enhanced operations would reduce the performance of learn-based methods. When searching in the large fingerprints database, if we input low-quality fingerprints extracted in CSI directly, the genuine match could not be found in the watch list.

This paper presents a combined coarse-to-fine method to rectify distorted latent fingerprints on curved objects. The robustness against multifarious interferences and the accuracy of correction are both we are concerned about. The traditional part could estimate the preliminary distortion fields in the coarse stage, which is rarely affected by interferences in CSI. Then, the region detector is used to detect the area with reliable extracted ridge features. Finally, the trained DCNN is introduced to modify the distortion field in the fine stage. Experimental results show better accuracy than other methods [13], [24], [25], especially on low-quality images. The comparison is based on the Shanghai Public Security Bureau (SPSB) test database containing over 20,000,000 fingerprints. Furthermore, the distorted fingerprint samples used in our paper are closer to forensic practice and differ significantly from other studies. We conducted 40 latent fingerprints left on curved objects (e.g., Coca-Cola bottles and doorknobs), smoked by 502 glue, enhanced with magnetic powder, and extracted by forensic photograph technology. The rank of genuine matches between original and rectified ones evaluates the effect of rectification.

This paper proposes a coarse-to-fine approach to rectify the latent distorted fingerprints extracted at a crime scene. The primary contributions of the proposed method are as follows:

(1) We propose a novel coarse-to-fine approach for rectifying latent distorted fingerprints on a curved object at crime scenes, leveraging a fusion of traditional pattern recognition methodology and deep neural network (DNN).

(2) We incorporate a deep convolutional neural network (DCNN) model to enhance the rectification performance, particularly when reliable ridge features can be extracted.

(3) The incorporation of traditional methodologies ensures the robustness of the algorithm in environments characterized by diverse interferences.

(4) Rectification can be achieved with a single distorted fingerprint, thus meeting the practical requirements of CSI investigations.

(5) The cumulative match characteristic (CMC) results demonstrate a significant enhancement, particularly in low-quality distorted images, within a database containing more than 20,000,000 fingerprints, providing strong evidence of improved performance in the forensic field.

The remainder of this paper is organized as follows. Section II reviews some studies related to distorted fingerprints. Section III presents our combined coarse-to-fine method in detail, and Section IV describes the experimental results and evaluates the performance of CMC compared with other methods [13], [24], [25]. Section V summarizes the paper and discusses future research directions.

II. RELATED WORKS

Researchers have proposed several methods to address the distortion in fingerprint images, which could be coarsely classified into three categories.

The first approach accounts for distortion in the acquisition stage. Dorai et al. [30], [31] and Fujii [32] observed a

video sequence of motion processing. The hardware rejects severely distorted records and measures the distortion across successive frames. It is desirable to detect and measure distortion during fingerprint acquisition automatically. Zhang et al. [33] proposed a novel real-time algorithm called block-based rolled fingerprint construction, which can evaluate the distortion in rolled fingerprints and rectify it. Due to the real-time attribute, these rectifications did not play a role in CSI.

In the second approach, the distortion is estimated during the matching stage. Increasing the bounding zone is popular for distortion-tolerant matching [18]. Most algorithms increase the size of the bounding box to tolerate the further apart matched minutiae pairs. Ratha et al. [12] proposed an algorithm combining a global rigid transform and a local tolerant window to address skin elasticity. Although the algorithms decrease the false rejection rate (FRR), this method leads to a higher false acceptance rate (FAR) as a side effect. Chen et al. [11] proposed a fuzzy similarity measure based on changeable bounding box size. The features concluded from genuine and impostor matches are applied in computing the probability to judge the matched minutiae pairs. It is a novel algorithm to cope with nonlinear distortion in fingerprint matching, balancing FRR and FAR, but it has obvious limitations in forensic science. Many fingerprints at a crime scene are latent and low quality. The algorithm will reject the minutiae extracted from heavily distorted ridges, while the fingerprints at a crime scene are frequently limited in the quantity of minutia. Kovacs-Vajna [34] introduced a fingerprint verification system based on the classic minutiae-matching method, with triangular matching to address distortion. It was proved valid in NIST SD4. A noticeable flaw of the method is that 40–60 minutiae are required, while it is uncommon for latent fingerprints at a crime scene.

Gu et al. [19] used a thin-plate spline (TPS) model to compare two minutiae sets extracted from fingerprints. They introduced the TPS function to address nonlinear deformation caused by elasticity, with excellent matching performance. Ross et al. [15] proposed a TPS model with ridge curve correspondences instead of minutiae correspondences, increasing the matching reliability. Lin and Kumar [16] presented a more robust TPS (RTPS) by minimizing transformed point localization errors to ensure the robustness of matching contactless and contact-based fingerprints. Such methods [15], [16], [19] have two primary limitations in application in forensic science. (1) The performance of the method highly depends on the number of impressions of the same finger. (2) The core of these methods is the TPS function, which has proved valid in rectifying elastic distorted fingerprints. This paper focuses on latent fingerprints left on a complex curved surface typical in CSI, not distortion caused by skin elasticity. Khongkraphan [23] introduced an efficient matching approach to address nonlinear distortion in fingerprint matching. It represents a fingerprint with minutiae features, including position, ridge orientation, and neighbor features.

The alignment method uses the data-clustering concept to find corresponding substructure pairs. Finally, a matching score could be computed to represent the similarity of two fingerprints. The approach performed better in FCV2002 and FCV2004 than in other approaches.

Recently, Rungchokanun and Areekul [29] applied a weight–distance model to address elastic deformation effects, assuming that the elastic deformation could not change the minutiae's order in the friction ridge flow; therefore, the closest neighbor minutia is more crucial than further ones. The proposed distance combines the Euclidean distance and the angle between the observed minutia's direction and its neighboring minutia. The model could cope with high-curved and highly deformed areas with additional features such as orientation and segmentation. Such approaches [23], [29] have significant obstacles in CSI. (1) These approaches are incompatible with the existing AFIS. (2) Evidence found in CSI is always low-quality latent fingerprints, which differ significantly from the samples used in these papers.

In the third approach, the distortion is removed before the matching stage. Anusha and Kumar [35] reported a CNN-based algorithm to detect and rectify latent distorted fingerprints. Despite achieving a high accuracy rate of 99% recognition rate, appropriate enhancement should be given to CNN first. It is not always available for CSI. Senior and Bolle [7] proposed a novel and interesting method for distortion removal, assuming that the ridge frequency within a normal fingerprint is constant. Compared to previous studies, the approach offers crucial accomplishments in single fingerprint processing; however, Wan and Zhou [14] reported that the ridge frequency is not constant within the entire fingerprint area. Lan et al. [20] proposed the preregistration of distorted fingerprints based on the correlation and orientation fields. The difference map between deformed and reference fingerprints estimates the deformation field based on the correlation and orientation fields. It has three primary steps. In the first step, the correlation is adapted to correct the entire translation. Second, the orientation field is used to correct nonrigid deformation. Finally, the registered fingerprint would be obtained by combining the correlation and orientation fields for iteration. The algorithm improves the matching accuracy in FCV2004 DB1, Tsinghua DF, and NIST SD27 compared with the Bloy and Verma [36], Tang et al. [37], and Fayad et al. [38] methods. Despite the better accuracy mentioned above, the reference fingerprint is the base of the method, making little sense in CSI because a single distorted fingerprint without reference is problematic.

Another nonrigid registration method is proposed by Lan et al. [22]. The novel approach combines the ridges' traditional minutiae and direction information, while the ridges' direction is frequently neglected or used indirectly. First, one query and one reference fingerprint were used to calculate their image field and difference map. Then, the deformation field is obtained using the model. Finally, the query fingerprint was rectified according to the deformation

field. Experiments have been conducted on four databases, including FCV2004 DB1, Tsinghua DF, NIST SD27, and NIST SD30. Despite the validity shown in the experiments, we must highlight that the method could not be applied in CSI because the criminal's identity is unclear, and no reference fingerprint is available when inputting a query fingerprint.

Si et al. [21] proposed a dense method to correct distorted fingerprints. It combines the advantages of the minutiae-based and image-based matching methods. The composite initial registration step decreases the distortion globally using the TPS model. The dual-resolution block-based registration step addresses the distortion locally. It has two main disadvantages. (1) Concluded from the CMC curve, the top 200 candidates' identification rate is under 0.5 on NIST SD27. (2) The method requires a reference fingerprint, severely restricting the application in CSI. Si et al. [13] suggested a novel algorithm to detect and rectify distorted fingerprints called the nearest-neighbor search. First, the orientation and period maps extracted from a reference image establish the distortion fields. Then, the distorted fingerprints could be rectified by geometric transformation using an estimated distortion field. The experimental results show recognition rate improvement in the distorted fingerprints in some public databases. The two disadvantages of this method are speed and practicability. The method performs poorly in NIST SD27, which was collected in CSI. Therefore, some researchers have made new progress.

Based on Si et al. [21] work, Guan et al. [26] proposed a novel dense method to estimate the distortion field. A self-reference relationship is constructed to finely estimate the detailed distortion patterns, so no reference fingerprint is required for rectification. A scaled mask is introduced in the feature extraction module, and the gradient of the estimated distortion field is presented in the loss function. The method achieves the state-of-the-art rectification performance in Tsinghua DF established by Si et al. [13]. The limitation of the method is that the training fingerprints are relatively clean; thus it may not be effective in the case of low-quality images. Cui et al. [27] proposed an attractive approach based on dense registration. The approach is a coarse-to-fine method containing two prime steps. First, minutiae matching roughly aligns the fingerprint. Second, a pixel-wise dense displacement field is computed for rectification. The matching experiments on FCV2004, Tsinghua DF, and NIST 27 show that the proposed approach outperforms previous dense registration methods in accuracy. Despite such improvements, the CMC curve on NIST27 indicates the application is still far from proof in forensics, for the top 20 cumulative match rate is not higher than 0.8 in only 258 pairs.

Gu et al. [19] optimized Si et al. [13] method in speed by introducing the Hough forest-based fingerprint pose estimation algorithm and support-vector-based fingerprint-distortion field estimation algorithm, more than 30 times faster than Si et al. [13] method with fair accuracy. However, the latent fingerprint database in NIST SD27 is omitted, which is quite significant in forensic science. Dabouei et al.

[24] proposed a more powerful approach using deep CNNs (DCNNs). Compared with Si et al. [13], Dabouei et al. [24] study reduces the consuming time considerably and improves the accuracy in FVC2004 DB1 and FVC2006 DB2. Two primary advantages could be concluded in the nearest-neighbor search method [13], the Hough forest and support vector method [19], and the DCNN-based method [24]. (1) A single distorted image is enough for rectification. (2) They are more precise than other methods in single-image distortion estimates.

Karabulut et al. [39] applied generative adversarial networks (GANs) in distorted fingerprint rectification. The model consists of two GANs in a cyclic fashion and trained in accordance. The database is provided for the research by GEYCE Biometrics and is not open for public access. Images displayed in the paper indicate distorted images are high-quality images that differ considerably from those extracted in CSI.

Zhengfang et al. [25] introduced a novel network in fingerprint identification last year called Siamese rectangular CNNs (SRCNNs). In the training phase, two fingerprint image pairs are simultaneously inputted into the network, and one pair is of the same person, whereas the other is not. In the convolution operation, the traditional square convolution kernel is replaced by a rectangular kernel because the rectangular kernel contains long curves, which can pass more friction features than the square kernel. The experimental results show that the accuracy of the SRCNN model is 4% higher than the compared method. Although the SRCNN improves the accuracy in NIST SD4, we must highlight that the existing results are insufficient to prove the validity in CSI because the capacity of the test database is only 2000 pair fingerprints.

Comprehensively considering the characteristics of the studies above, Dabouei et al. [24] model, Si et al. [13] algorithm, and Zhengfang et al. [25] network are selected as comparative methods to evaluate our method. Our approach shares the advantages of previous methods [13], [19], [24], [25] and can deal with a single distorted fingerprint image in CSI. Besides, our method overcomes the most noticeable defects in these methods [13], [19], [24], [25] and robustness in various interferences of latent fingerprints in CSI.

III. METHODOLOGY

This paper proposes a new method to rectify distorted fingerprints, combining traditional pattern recognition and deep neural networks. We propose a coarse-to-fine approach to address the latent distorted fingerprints on a curved object at a crime scene. It has three primary steps. First, nonlinear deformation caused by curved surfaces is estimated using two standard scales affixed to the curved object, and the measure is robust to various interferences commonly met in CSI. Second, similar to Dabouei et al. [24] method, a DCNN model is introduced to estimate the distortion field of the input image. The final step combines the advantages of both approaches. Fig. 1 shows a flowchart of the proposed rectification.

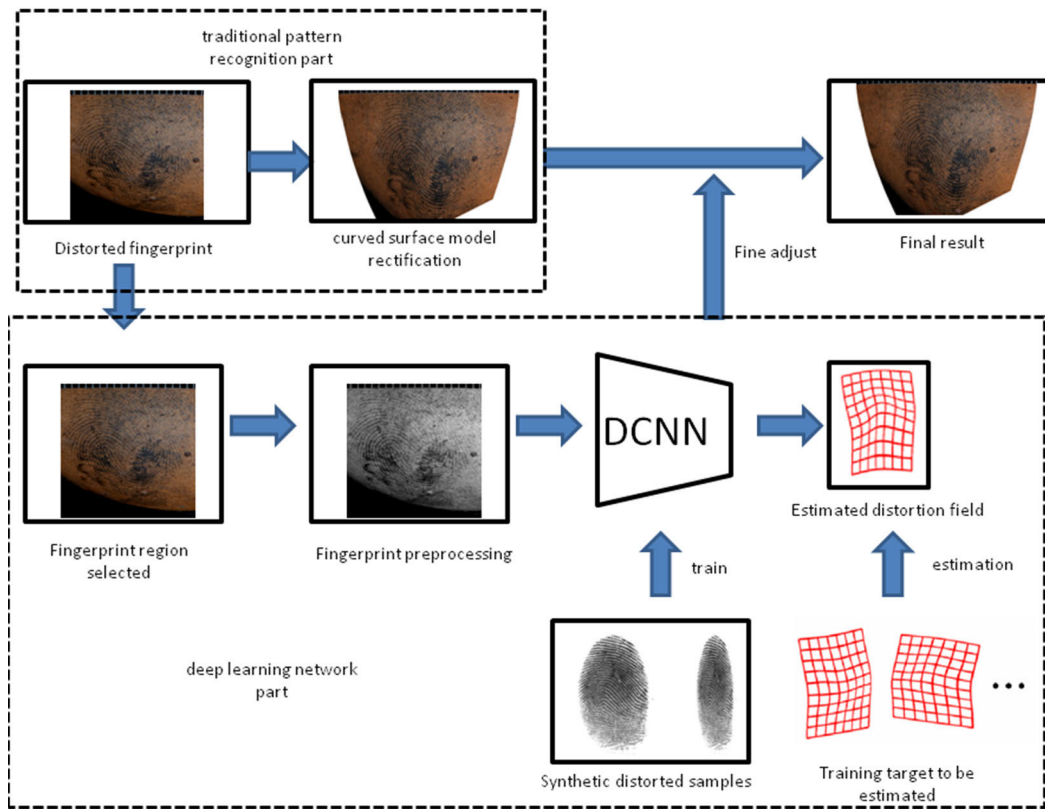


FIGURE 1. Flowchart of the proposed distorted fingerprint rectification method.

The dashed line at the top shows a part of the traditional pattern recognition, which is the coarse stage in our approach. The latent fingerprints would be enhanced and extracted by forensic techniques. Then, the preliminary distortion field would be estimated based on the curved surface model. The distortion field would be divided into horizontal and vertical parts. In general, the distortion field is determined by the position in the image, which is estimated by standard scales attached to the surface. The dashed line at the bottom shows a part of the deep learning network. This part is inspired by the approach proposed by Dabouei et al. [24]. The nonlinear transformations are learned by DCNN in the training phase. We used 401,000 synthetic distorted fingerprint samples to train the network, similar to the operation conducted by Dabouei et al. [24]. Due to the significant gap between training samples and latent fingerprints extracted in CSI, the traditional and network parts should be combined to improve the rectification performance. The local distortion field of each part would be computed to judge the mode and parameters of fusion. The low similarity of the two parts indicates extracted ridge features influenced by interferences seriously. Then, the rectification results of DCNN would be discarded. In contrast, high similarity reveals ridge features extracted well in the local block. Then, the estimated distortion field could be modified by DCNN to improve rectification performance.

A. SIMULATION SAMPLES AND TEST DATABASE

In this paper, we conducted 40 latent fingerprint samples on multiple objects, including eggs, Coca-Cola bottles, mouse buttons, and doorknobs. Fig.2 shows two simulation samples used in this paper. To meet the realistic demand of forensics, the extraction progress refers to practical work in CSI, smoked by 502 glue, enhanced with magnetic powder, and extracted using a specialized optical method. Furthermore, the ridge condition is closer to reality, the interruption of the ridge, the vagueness of the core region, and background interference. However, the public fingerprint databases used in other studies are often inked impressions, which are too idealized for forensic science. Fig.3 shows two test samples used in Dabouei et al. [24] method.

(a) Latent fingerprint on an egg, enhanced with magnetic powder, (b) latent fingerprint left on a bottle, smoked with 502 glue.

(a) Slight distortion sample, (b) severe distortion sample.

In this paper, the Shanghai Public Security Bureau fingerprint (SPSB) fingerprint test database was selected to verify the performance of rectification. It contains over 20,000,000 fingerprints, while the largest typically used database, NIST SD14, only comprises 27,000 fingerprints. The database consists of inked fingerprints of people with criminal records or other reasons prescribed by law, scanned or photographed in the JPG or BMP format with high image quality.

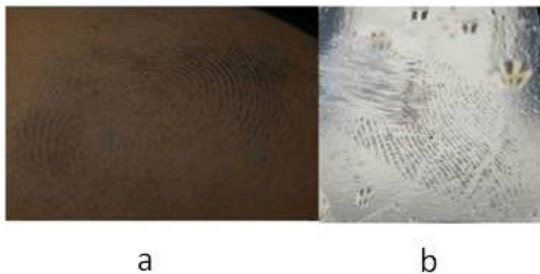


FIGURE 2. Samples of simulation fingerprints in this paper.



FIGURE 3. Two samples of the testing fingerprint in Ali Dabouei's approach.

Generally, planar and roll samples would be collected for each fingerprint to increase the hit rate. For each image, the AFIS would extract fingerprint features automatically, such as the pattern of the core region, center point, and pattern triangular region. In order to ensure the quality of the input image, extracted features would be manually reviewed before finally entering the database. Some samples of the SPSB fingerprint test database are shown in Fig.4.

In our paper, inked fingerprint and simulated latent fingerprint images will be conducted first. Then, the inked image would be put into the SPSB fingerprint test database as samples for comparison. Next, original or rectified images would be searched in the database containing more than 20,000,000 fingerprints as a query fingerprint. As a result, the watch list would be returned by AFIS, and the rank of genuine matches would be checked. In forensic practice, the rank of the genuine match and the capacity of the database are negatively correlated. For low-quality fingerprints, the phenomenon is more obvious. The rank of the genuine match would drop dramatically with the increasing capacity of the database, which would lead to a missed result. Instead of the score, the rank is much more crucial for matching in forensic science because experts would check the top 50 candidates in the watch list to determine whether there are genuine matches. Therefore, the CMC curve is typically used to compare the fingerprint-matching accuracy. In the CMC curve, the ordinate is the cumulative match rate, and the abscissa is the rank. For example, the point (50, 0.9) means the rate of genuine match in the top 50 candidates in the watch list is 0.9. The database capacity in this paper is much larger than any other test database in the references; therefore, the CMC curve in this test database is more convincing in the forensic field.

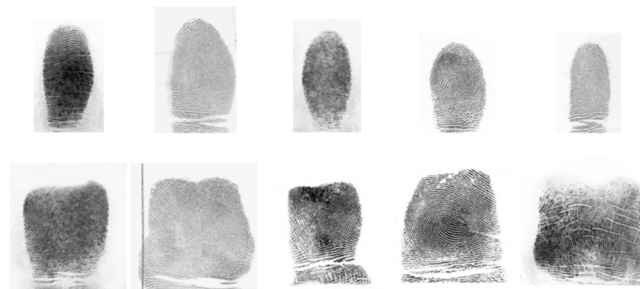


FIGURE 4. Samples in the SPSB fingerprint test database used in our paper.

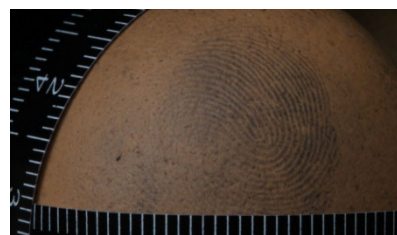


FIGURE 5. Sample of standard scales attached to the curved object surface.

B. ALGORITHM ARCHITECTURE

1) TRADITIONAL PATTERN RECOGNITION PART

In this paper, the input image is distorted fingerprints on a curved surface. Two standard scales should be attached to the curved surface of the objects for rectification (Fig.5). The curved object is regarded as curve L_2 generated by rotation along curve L_1 , and the sketch is shown in Fig.6

The horizontal red dashed line represents L_1 , and the vertical red dashed line represents L_2 .

The interval between the scales should be even in the image without distortion, and the smaller interval suggests a greater distortion degree. The first rectification step is computing the horizontal distortion field in L_1 using the horizontal scale. Let c_n denote an array prepared to match. c_n is calculated using Equation 1, and the sketch map is shown in Fig.7.

$$c_n = b_n + a_n + b_{n+1} \tag{1}$$

b_n and b_{n+1} represent the interval between adjacent scales, and a_n is the width of the scale.

The least deformation position in L_1 is determined by solving the following formula:

$$\arg \max_t \text{balance} \left(\frac{\sum_1^{t-1} c_n}{\sum_{t+1}^n c_n} \right) \tag{2}$$

where t denotes the maximum projection position, the candidates of the maximum projection position comprise the largest part of c_n ; a lower bound is 99% of the maximum element. Function $\text{balance}()$ returns the minimum of the input function and its reciprocal. Equation 2 ascertains the position with the least deformation in L_1 . Next, an optimal match surface with a fixed radius is determined by solving the

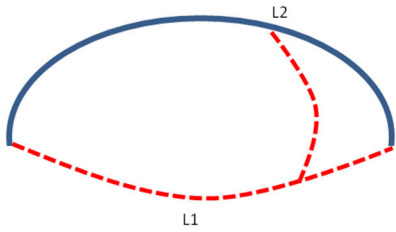


FIGURE 6. Sketch of the standard scales attached to the surface.

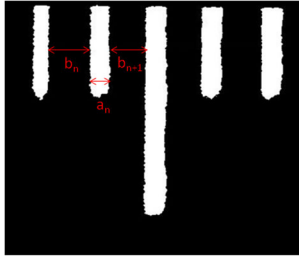


FIGURE 7. Schematic diagram of computing c_n .

following equation:

$$\arg \min_{\theta} \|c_n - \text{match}(\theta, t)\| \quad (3)$$

Function $\text{match}()$ means matching a curved surface with a fixed radius in position t , $\|\cdot\|$ counts the norm-2 distance, and θ denotes the curvature radius. Fig.8 shows an intuitive presentation.

The solid blue line refers to the curved object surface, and the red dashed line shows the optimal match surface computed using Equation 3. The red dot t is the position determined by Equation 2.

In CSI, curved objects with latent fingerprints do not always have a fixed radius. The matching surface should be modified based on Equation 3 as follows:

$$\arg \min_{A,B} \|c_n - (\text{match}(\theta, t) + A \times \theta + B \times \theta^2)\| \quad (4)$$

A and B are coefficients based on the result of Equation 3. Given a set of discrete horizontal distortion fields obtained by Equation 4, serialization is the following step to rectification. The discrete horizontal distortion field could be transformed into continuous functions, as in Formula 5. The explanatory drawing is shown in Fig. 9

$$\frac{\int_{\alpha}^{\theta_2} \cos \theta d\theta}{\int_{\theta_1}^{\alpha} \cos \theta d\theta} = \frac{L_l}{L_r} \quad (5)$$

The blue curve refers to the object's surface, θ_1 and θ_2 are angles of adjacent scales in the object's surface, and α is an arbitrary point in the arc. The red dashed line represents the projection results for fingerprints extracted by the photograph originally. Suppose α is an arbitrary point in L_1 , the horizontal distortion field $\beta_h(\alpha)$ could be estimated as follows:

$$\beta_h(\alpha) = \sqrt{1 - \left(\frac{L_r \times \sin \theta_2 + L_l \times \sin \theta_1}{L_l + L_r}\right)^2} + A \times \theta_x + B \times \theta_x^2 \quad (6)$$

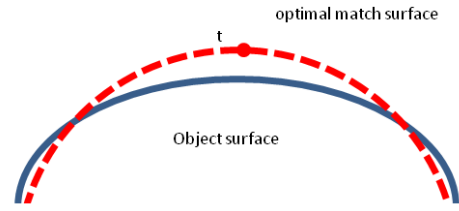


FIGURE 8. Sketch map of the matching process.

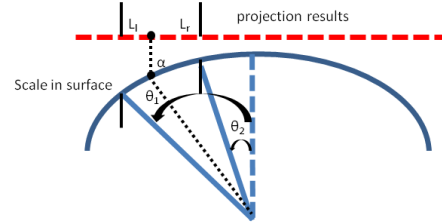


FIGURE 9. Draft picture of the serialization step.

All parameters except θ_x in the above formula can be indexed in Equation 4, where θ_x is determined by the angle corresponding to the adjacent scale in Equation 5. Thus far, the horizontal distortion field in L_1 has been estimated. The vertical distortion field in L_2 takes a similar approach, and the results are recorded as $\beta_v(\alpha)$.

Then, generalizing the computation of the distortion field to an arbitrary point in the curved surface is another critical point for rectification. The distortion field can be determined using L_1 and L_2 through a curved surface model. To the horizontal distortion field, the curved objects can be viewed as a vertical stack similar to L_1 . The horizontal distortion field $\beta_h(\tau)$ at arbitrary point τ is described as formula follows:

$$\beta_h(\tau) = \text{transform}_h(x, y, \beta_h(\alpha)) \quad (7)$$

where x and y are coordinates of τ , and the function $\text{transform}_h()$ means mapping relationship corresponding to the horizontal distortion field $\beta_h(\alpha)$ in L_1 . An intuitive explanation is shown in Fig.10

(a) The blue curves refer to the object surface in different vertical positions, similar to the corresponding relationship between A_1 to B_1 , A_2 to B_2 , and A_3 to B_3 . (b) The ratio of similitude is decided by r_2 divided by r_1 . The vertical dashed line represents the position of t determined by Equation 2, and the solid curved line L_2 is the vertical distortion field. Then, r_1 is the distance between t and L_2 in the vertical position of L_1 , and r_2 is the distance between t and L_2 in the vertical position of the arbitrary point in the curved surface.

To the vertical distortion field, the curved objects could be viewed as a horizontal stack of curve clusters transformed from L_2 . The vertical distortion field $\beta_v(\tau)$ at arbitrary point τ is described as equations follow:

$$k = \frac{\int \sin \cos^{-1} L_1}{\int \sin \cos^{-1} R} \quad (8)$$

$$\beta_v(\tau) = \text{transform}_v(x, y, k, \beta_v(\alpha)) \quad (9)$$

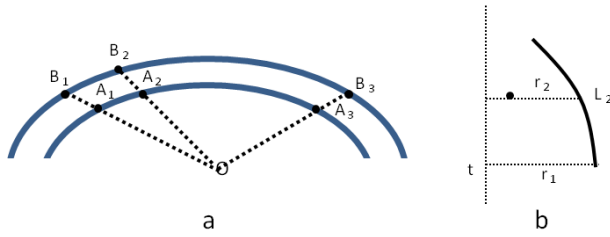


FIGURE 10. A diagram of the function $transform()$.

In Equation 8, L_1 and R represent the horizontal distortion field of L_1 and the fixed radius, respectively, and k is the ratio used in Equation 9. Similar to Equation 7, x and y are the coordinates of the arbitrary point, and function $transformv()$ is the mapping relationship corresponding to the vertical distortion field $\beta_v(\alpha)$ in L_2 . An intuitive explanation is shown in Fig. 11.

(a) The solid blue curve is the horizontal distortion field $\beta_h(\alpha)$ in L_1 , and the red dashed line refers to a virtual curve with a fixed radius. The distance between the arbitrary point and curved surface in the depth dimension is r_1 , when it comes to a virtual curve with a fixed radius, namely r_2 . (b) The red dashed line is a vertical distortion field $\beta_v(\alpha)$ in L_2 , and the blue solid line refers to the result of the transformed vertical distortion field L_2' . The L_2' can be regarded as a stretch transformation from L_2 , with the ratio decided by r_1 divided by r_2 .

2) DCNN PART

Learning-based models become a novel rectification approach in recent years. The supervised learning method could provide prior knowledge during the training process, which improves the generalization capability of the method [40], [41]. Some references have reported that the performance of fingerprint rectification could be improved with the DCNN introduced.

In the field of forensic science, meeting the criteria for the reference fingerprints cited in the literature ([15], [16], [19], [20], [22], [35]) is challenging. Single latent distorted fingerprints are frequently encountered in CSI. The DCNN part of our method is inspired by the rectification approach proposed by Dabouei et al. [24], due to the ability to handle a single image and excellent performance in public databases such as FVC2004 and FVC2006. The results reported by Dabouei et al. [24] indicate that such a designed DCNN could improve the rectification performance compared with other methods in fingerprints with little interference. In our paper, the DCNN part acts as a fine stage to modify the distortion field estimated by the coarse stage. The database used in the training phase, the generation of synthetic distorted fingerprints, and the training methods are all the same as in Dabouei et al. [24]. We generated a distorted synthetic database using 1033 normal fingerprints from the BioCOP 2013 database. Each normal sample was transformed into 400 distorted images by sampling the two

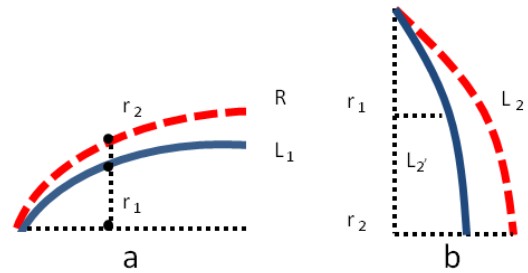


FIGURE 11. A diagram of the function $transformv()$.

principal distortion components extracted from the Tsinghua database. We matched minutiae pairs between original and distorted samples to extract displacement due to distortion. Based on such matching operation, it is possible to represent distortion as displacement of corresponding minutiae on the original grid and distorted grid as follows equation:

$$d_i = x_i^D - x_i^N \quad (10)$$

where d_i represents the displacement of minutia for the i th pair of distorted and corresponding normal fingerprints. The distortion field could be approximated using the PCA method [42], [43] as the following equation:

$$\hat{d} = \bar{d} + \sum_{i=1}^t c_i \sqrt{\lambda_i} e_i \quad (11)$$

In equation 11, t is the number of selected principal components, c_i is the coefficient of the corresponding eigenvector component, λ_i is the eigenvalue and e_i is the corresponding eigenvector component. First, two significant eigenvectors of distortion were used to generate synthetic samples for training. Some examples of synthetic distorted samples are shown in Fig. 12. To verify the validity of Dabouei et al. [24] work, the receiver operating characteristic (ROC) curve of matching experiments is shown in Fig. 13-14. As the experiments conducted and reported in Dabouei et al. [24] work, original fingerprints rectified by Si et al. [13] were selected as comparison results in the experiment. The compared result conducted on the Tsinghua DF database (320 fingerprint videos) and FVC 2004 database (3,520 fingerprints) indicates that DCNN could get excellent performance under appropriate conditions.

The DCNN minimizes the norm-2 distance between the coefficients and outputs. Our method uses input-distorted images to train the DCNN by 40 epochs. Each epoch comprised 6265 iterations, with a batch size equaling 64. The Adam optimization method uses $\beta = 0.5$ and learning rate $= 10^{-4}$. All layers except the last one are convolutional. The input image is $256 \times 256 \times 1$. Each layer except the last one comprises convolution, batch normalization, rectified linear unit (ReLU), and max pooling with strides equal to two. The detailed properties of the network are shown in Table 1. All layers except the last one comprise convolution (Conv), batch normalization (BN), ReLU, and max pool (MP). All max-pooling operations are 2×2 with a stride of two. All

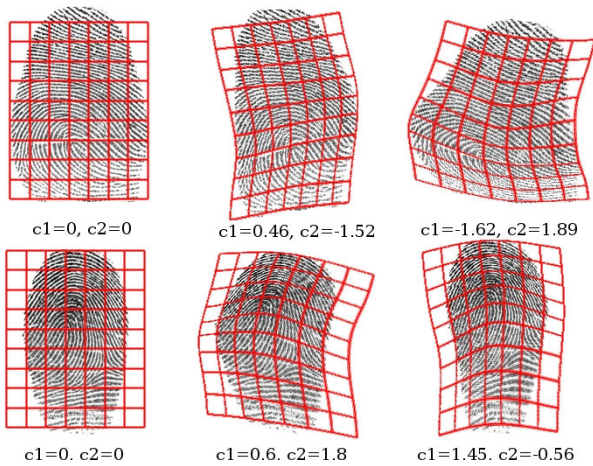


FIGURE 12. Examples of synthetic distorted fingerprints generated for training the network.

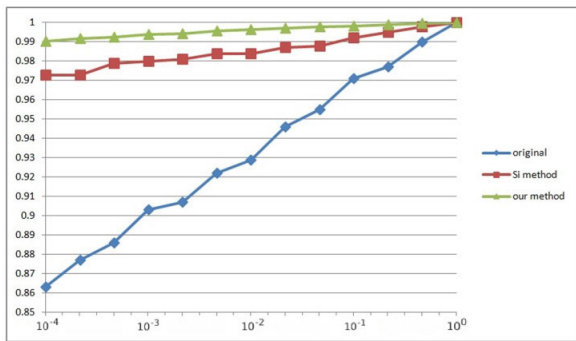


FIGURE 13. Compared results conducted on the Tsinghua DF database.

convolution strides are one, and all inputs to convolutions are padded to have the same size outputs. Different from the inked impressions in Dabouei et al. [24] approach, the distorted latent fingerprints in our paper are extracted according to the CSI standard. Preprocessing must meet the requirements of the DCNN model.

In this paper, our focus is the rectification performance of latent fingerprints, especially low-quality images. Different kernel sizes, including 3×3 , 5×5 , and 7×7 with the same channels are tested to determine the optimal size. The compared results and analysis are shown in Section IV.

3) COMBINATION PART

Traditional pattern recognition and DCNN play different roles in rectifying distorted latent fingerprints. For conventional pattern recognition, robustness is a prominent advantage. As reported by Si et al. [13], the complex background of latent fingerprints interferes with period and orientation map extraction from images. Low-quality images lead to unsuccessful rectification in NIST SD27. In Dabouei et al. [24] approach, the test databases are inked fingerprints. The traditional part is robustness to latent fingerprints, which can estimate the distortion field reliably. For DCNN, accuracy is the key advantage compared with other methods, and it

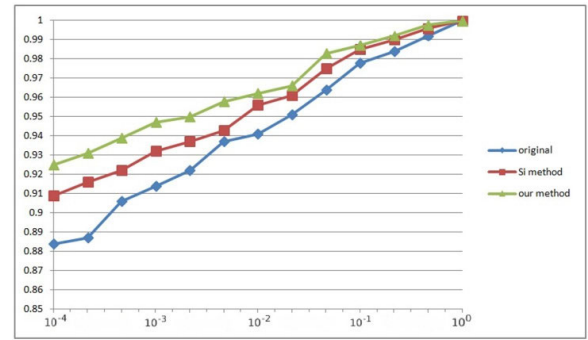


FIGURE 14. Compared results conducted on FVC2004-DB1-4 set A.

TABLE 1. Architecture of DCNN.

Layer	Type	Kernel size	Input size	Output size
1	Conv,BN, ReLU,MP	$3 \times 3 \times 32$	$256 \times 256 \times 1$	$128 \times 128 \times 32$
2	Conv,BN, ReLU,MP	$3 \times 3 \times 64$	$128 \times 128 \times 32$	$64 \times 64 \times 64$
3	Conv,BN, ReLU,MP	$3 \times 3 \times 64$	$64 \times 64 \times 64$	$32 \times 32 \times 64$
4	Conv,BN, ReLU,MP	$3 \times 3 \times 128$	$32 \times 32 \times 64$	$16 \times 16 \times 128$
5	Conv,BN, ReLU,MP	$3 \times 3 \times 256$	$16 \times 16 \times 128$	$8 \times 8 \times 256$
6	Conv,BN, ReLU,MP	$3 \times 3 \times 512$	$8 \times 8 \times 256$	$4 \times 4 \times 512$
7	Conv,BN, ReLU,MP	$3 \times 3 \times 1024$	$4 \times 4 \times 512$	$2 \times 2 \times 1024$
8	Conv,BN, ReLU,MP	$3 \times 3 \times 2048$	$2 \times 2 \times 1024$	$1 \times 1 \times 2048$
9	Conv	$1 \times 1 \times 2$	$1 \times 1 \times 2048$	$1 \times 1 \times 2$

gains the best rectification result when the ridge map can be extracted reliably. Our method was designed as a coarse-to-fine process, combining the advantages of both approaches. DCNN is used to estimate the distortion field in a dependable ridge region; otherwise, the traditional part takes over the job. Since the input image of DCNN is 256×256 , we first segment the image into 32×32 blocks. Then, the matching relationship between the grid of the output of DCNN and traditional works can be established. The draft picture is shown in Fig. 15.

(a) Four 32×32 matching blocks in the DCNN input image (b) Four 32×32 matching blocks in the output image rectified by DCNN (c) Four 32×32 matching blocks in the output image rectified by the traditional part.

The combination depends on the similarity of the matching blocks between the DCNN model and the traditional part. A low similarity indicates that the image quality does not meet the requirement of the trained DCNN. However, a high similarity implies that the accuracy of DCNN can achieve a better effect than the traditional part. The parameter γ of similarity could be defined as the following equation:

$$\gamma = \frac{\vec{r}_1 * \vec{r}_2}{|\vec{r}_1|^2 \times |r_2|^2 - \vec{r}_1 * \vec{r}_2} \times \frac{\vec{r}_3 * \vec{r}_4}{|\vec{r}_3|^2 \times |r_4|^2 - \vec{r}_3 * \vec{r}_4} \quad (12)$$

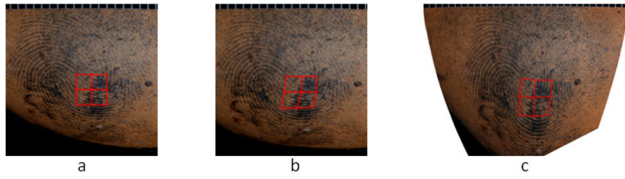


FIGURE 15. Draft picture of four 32×32 matching block mapping.



FIGURE 16. A sketch map of diagonal vectors in similarity computing.

where \vec{r}_1 , \vec{r}_2 , \vec{r}_3 , and \vec{r}_4 denote the diagonal vectors of the matching blocks, $*$ is the inner product of vectors, and γ represents the similarity threshold. The sketch map is shown in Fig. 16.

(a) The 32×32 matching block in the output image rectified by DCNN; \mathbf{r}_1 and \mathbf{r}_3 are diagonal vectors (b) The 32×32 matching block in the output image rectified by traditional parts; \mathbf{r}_2 and \mathbf{r}_4 are diagonal vectors.

Different matching blocks, including 16×16 , 32×32 , and 64×64 are compared to determine the optimal size. Besides, the similarity threshold conducts the same comparison with the range from 0.7 to 0.9. Based on the results shown in section IV, the matching block is selected 32×32 , and the similarity threshold is set to 0.8 in our method.

If the similarity does not reach the threshold, the traditional part takes over the rectification, and DCNN will not be accepted in the block. However, the rectification of DCNN can be used for fine adjusting in the block. The principle of fine adjusting is modifying the internal distortion field with a matching block shape invariable. The internal transform in the block follows the equation:

$$(x'_1, y'_1) = \text{transformco}(\text{transformob}((x_1, y_1))) \quad (13)$$

In the above equation, (x'_1, y'_1) denotes the coordinates after internal adjusting, and (x_1, y_1) represents the coordinates of traditional part addresses. The function $\text{transformob}()$ refers to the transformation from the ordinal number in the rectification block of the conventional part to that in the rectification block of the DCNN. Function $\text{transformco}()$ is the transformation from the coordinates in the rectification block of DCNN to those in the rectification block of the traditional part. The abridged general view is shown in Fig. 17

(a) The blue dashed line is the general shape of 32×32 blocks rectified by the traditional part, the tiny red square is the distortion field in each pixel in the block, and the solid black box represents the ordinal result of the arbitrary point before $\text{transformob}()$, and the black dotted box represents the

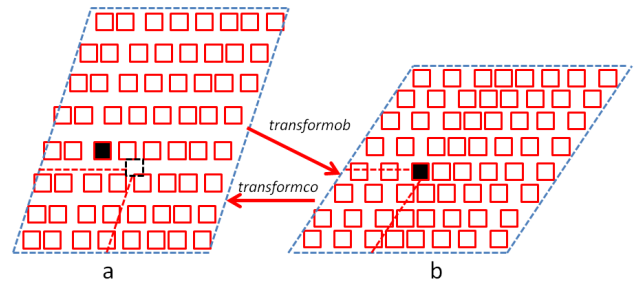


FIGURE 17. Abridged general view of fine adjusting.

coordinate results after $\text{transformco}()$. (b) The blue dashed line is the general shape of 32×32 blocks rectified by DCNN, the tiny red square is the distortion field in each pixel in the block, and the solid black box represents the ordinal result after $\text{transformob}()$. The solid black box mapping from (a) to (b) is the function $\text{transformob}()$ that guarantees a constant ordinal relationship. The mapping between the solid black box and black dotted box from (b) to (a) is a function $\text{transformco}()$ that guarantees a constant length percentage in each coordinate axis.

Due to the similarity of the adjacent distortion field, the mapping from (x_1, y_1) to (x'_1, y'_1) is modified by the following formula:

$$\begin{cases} x''_1 = (x'_1 - x_1) \times \omega_i + x'_1 \\ y''_1 = (y'_1 - y_1) \times \omega_i + y'_1 \end{cases} \quad (14)$$

where (x''_1, y''_1) denotes the final coordinates, and ω_i represents the coefficient decided by the satisfied similarity threshold in the connected 32×32 blocks. The abridged general view is shown in Fig. 18.

The center box denotes 32×32 blocks under transform computing, and the connected boxes indicate the adjacent 32×32 blocks. (a) The satisfied threshold of similarity equals 1, then $\omega_1 = 0.25$. (b) The satisfied threshold of similarity equals 2, then $\omega_2 = 0.5$. (c) The satisfied threshold of similarity equals 3, then $\omega_3 = 0.75$. (d) The satisfied threshold of similarity equals 4, then $\omega_4 = 1$.

IV. EXPERIMENT RESULTS

A. OPTIMIZATION PARAMETER EXPERIMENTS

Control variable experiments were conducted to determine our method's optimal parameters based on the SPSB test database. The same minutiae were selected manually in different images of the same fingerprint, similar to when fingerprints are extracted in CSI. The database contained more than 20,000,000 fingerprints. Different matching block sizes (16×16 , 32×32 , 64×64), different kernel sizes of DCNN (3×3 , 5×5 , 7×7), and different similarity thresholds (0.7, 0.75, 0.8, 0.85, 0.9) were used to test one by one combination on the SPSB test database. Tables and CMC curve are demonstrated as follows.

Fig. 19 and Table 2 show the results of different matching block sizes with the same kernel size (3×3) and the same

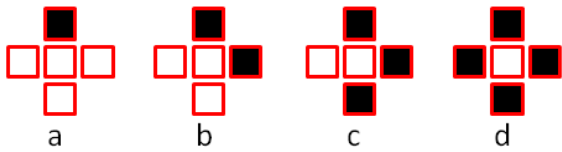


FIGURE 18. The abridged general view of coefficient adjust.

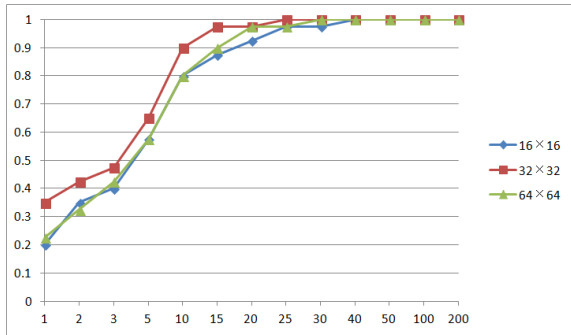


FIGURE 19. The CMC curve of different block sizes.

similarity threshold (0.8). The result of 64×64 is fairly proximate to that obtained solely by the traditional module. It can be explained that the block size of 64×64 occupies an excessive portion of the entire fingerprint image (256×256). Consequently, the segmentation of the image is too coarse, and the similarity threshold could hardly be satisfied. The result of 16×16 is usually slightly worse than that of 64×64 . This can be attributed to the relatively diminutive size of 16×16 within the entire image. In low-quality fingerprints, mixed interference would significantly impact ridge features extracted by a learning-based model. The above phenomena generally exist in combinations of different kernel sizes (5×5 , 7×7) and different similarity thresholds (0.7, 0.75, 0.85, 0.9).

Fig. 20 and Table 3 show the results of different kernel sizes with the same matching block size (32×32) and the same similarity threshold (0.8). All the kernel sizes could improve the genuine match compared to the original images, especially in low-quality fingerprints. It could be explained that severe deformation has been modified in the coarse stage. In general, small kernel size performs better than large kernel size. It could be explained that small kernel size brings out the advantage of deep learning networks. Distortion field estimated more precise with small kernel size in the region ridge information extracted reliably. The above phenomena generally exist in different matching block sizes (16×16 , 64×64) and different similarity thresholds (0.7, 0.75, 0.85, 0.9) combinations.

Fig. 21 and Table 4 show the result of different similarity thresholds with the same kernel size (3×3) and the same matching block size (32×32). It could be explained that the appropriate similarity threshold obtains optimal performance for the coarse stage and fine stage combined well. Different from other parameters, the change of matching block size significantly affects the tendency of CMC curves, while the

TABLE 2. The compared rank of genuine matches of different matching block.

Number	16×16	32×32	64×64
1	23	10	18
2	2	1	1
3	1	1	1
4	4	1	3
5	3	1	3
6	2	4	4
7	36	23	28
8	2	1	2
9	11	12	12
10	7	6	6
11	1	1	1
12	7	5	5
13	9	4	7
14	16	13	16
15	25	8	17
16	5	5	5
17	2	2	2
18	5	5	4
19	6	6	6
20	1	1	1
21	3	1	1
22	7	5	7
23	14	7	8
24	5	6	7
25	19	14	15
26	1	1	1
27	6	3	4
28	7	7	7
29	8	6	6
30	10	7	13
31	1	1	1
32	1	1	1
33	4	4	4
34	2	2	3
35	12	7	12
36	1	1	1
37	1	1	2
38	5	1	6
39	4	3	3
40	2	2	2

kernel size doesn't. Small kernel size achieves a slight advantage over large size in all the comparison results. Results of the influence of matching block size are shown in Fig. 22-23 and Table 5-6.

Fig. 22 and Table 5 show the result of different similarity thresholds with the same kernel size (3×3) and the same matching block size (64×64). The rank of genuine match is almost constant with various similarity thresholds. It could be explained that the 64×64 matching block size is too rough for the entire fingerprint image (256×256). Interference seriously disturbs the ridge features in almost matching blocks, leading to a significant gap between diagonal vectors between the coarse and fine stages. Changing the similarity threshold could not be enough to locate those blocks that should be modified.

Fig. 23 and Table 6 show the different similarity thresholds with the same kernel size (3×3) and the same matching block size (16×16). With the increase of similarity threshold, the performance of rectification rises rapidly at first and then tends to be stable. It could be explained that the 16×16 matching block size is too tiny for the entire fingerprint

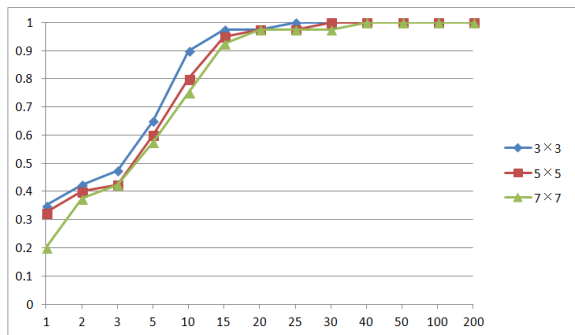


FIGURE 20. The CMC curve of different kernel sizes.

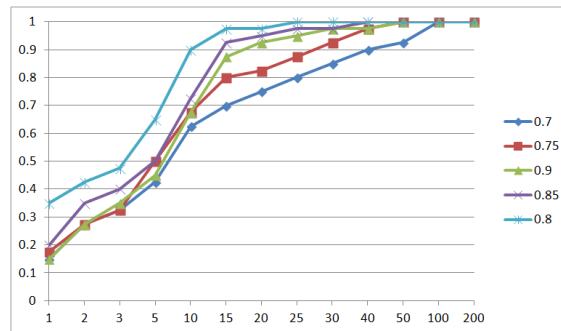


FIGURE 21. The CMC curve of different thresholds of combination.

TABLE 3. The compared rank of genuine matches of different kernel size.

Number	3×3	5×5	7×7
1	10	14	15
2	1	1	1
3	1	1	1
4	1	1	2
5	1	1	2
6	4	4	4
7	23	28	33
8	1	1	2
9	12	12	11
10	6	6	7
11	1	1	1
12	5	5	4
13	4	8	13
14	13	17	18
15	8	11	14
16	5	5	5
17	2	3	3
18	5	4	2
19	6	5	5
20	1	1	1
21	1	1	1
22	5	7	8
23	7	10	11
24	6	7	8
25	14	15	19
26	1	1	1
27	3	4	5
28	7	7	7
29	6	6	5
30	7	11	12
31	1	1	1
32	1	1	2
33	4	6	7
34	2	2	3
35	7	12	12
36	1	1	1
37	1	1	1
38	1	2	6
39	3	5	8
40	2	2	2

TABLE 4. The compared rank of genuine matches of different threshold.

Number	0.7	0.75	0.8	0.85	0.9
1	54	22	10	17	25
2	1	1	1	1	2
3	5	3	1	3	3
4	9	7	1	2	4
5	6	4	1	1	1
6	4	4	4	4	4
7	77	42	23	35	41
8	18	11	1	1	1
9	23	15	12	10	10
10	3	5	6	6	8
11	2	2	1	2	2
12	6	6	5	8	9
13	20	15	4	4	13
14	12	13	13	15	15
15	35	31	8	12	13
16	29	18	5	9	10
17	1	2	2	2	3
18	5	5	5	7	7
19	6	6	6	6	6
20	1	1	1	1	1
21	3	3	1	2	6
22	5	5	5	5	4
23	14	12	7	12	14
24	9	6	6	5	4
25	43	39	14	14	15
26	1	1	1	1	1
27	14	4	3	7	7
28	7	7	7	10	11
29	22	9	6	13	16
30	30	23	7	9	10
31	1	1	1	1	1
32	1	1	1	1	2
33	7	6	4	12	16
34	2	2	2	3	3
35	68	27	7	11	12
36	1	1	1	1	1
37	2	1	1	2	2
38	38	30	1	24	28
39	7	5	3	11	15
40	2	2	2	2	2

(256 × 256). The advantage of robustness acquired from the coarse stage is not fully exploited. Some disturbed blocks are also corrected by the deep learning module, which reduces the rank of genuine matches. When the similarity threshold reaches the specific value, the CMC curve tends to be stable for the method degenerates into a rough module working alone.

We clearly find out that the best performance under the condition of 64 × 64 matching block size and 16 × 16 matching block size is not as good as the optimal result with the small kernel size (3 × 3) and appropriate matching block size (32 × 32). So, the parameters in our approach are set as 32 × 32 (matching block size), 3 × 3 (kernel size), and 0.8 (similarity threshold).

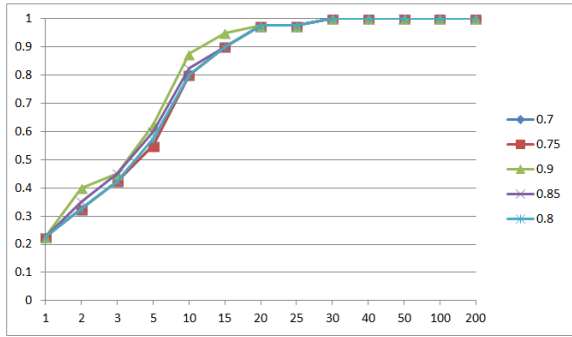


FIGURE 22. The CMC curve of different thresholds of combination.

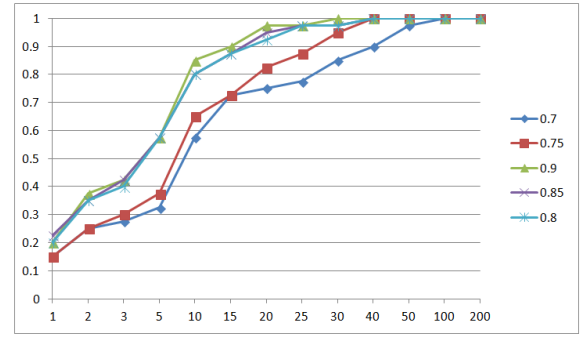


FIGURE 23. The CMC curve of different thresholds of combination.

TABLE 5. The compared rank of genuine matches of different threshold.

Number	0.7	0.75	0.8	0.85	0.9
1	18	18	18	17	15
2	1	1	1	1	1
3	1	1	1	1	1
4	3	3	3	3	3
5	4	3	3	3	2
6	4	4	4	4	4
7	30	30	28	28	28
8	2	2	2	2	2
9	13	13	12	11	10
10	6	6	6	6	7
11	1	1	1	1	1
12	6	6	5	5	4
13	7	7	7	7	7
14	16	16	16	16	16
15	17	17	17	16	12
16	5	5	5	5	5
17	2	2	2	2	2
18	4	4	4	2	2
19	8	6	6	6	5
20	1	1	1	1	1
21	1	1	1	1	1
22	7	7	7	7	6
23	8	8	8	8	8
24	7	7	7	7	7
25	15	15	15	15	15
26	1	1	1	1	1
27	4	4	4	4	4
28	7	7	7	7	7
29	6	6	6	5	5
30	15	15	13	11	9
31	1	1	1	1	1
32	1	1	1	1	2
33	4	4	4	4	4
34	3	3	3	3	2
35	12	12	12	11	10
36	1	1	1	1	1
37	2	2	2	2	1
38	7	6	6	6	6
39	3	3	3	3	3
40	2	2	2	2	2

TABLE 6. The compared rank of genuine matches of different threshold.

Number	0.7	0.75	0.8	0.85	0.9
1	42	30	23	20	17
2	2	2	2	1	1
3	8	4	1	1	1
4	11	9	4	4	4
5	9	8	3	3	3
6	4	4	2	2	2
7	63	39	36	33	29
8	20	17	2	2	2
9	19	13	11	11	10
10	8	8	7	6	6
11	2	1	1	1	1
12	6	6	7	7	6
13	27	16	9	8	7
14	15	15	16	16	16
15	29	26	25	22	18
16	33	22	5	5	5
17	1	2	2	2	2
18	8	6	5	5	4
19	8	6	6	6	6
20	1	1	1	1	1
21	3	3	3	3	2
22	7	7	7	7	6
23	18	18	14	14	13
24	8	7	5	5	5
25	36	29	19	16	15
26	1	1	1	1	1
27	11	10	6	6	6
28	7	7	7	7	7
29	25	16	8	8	7
30	28	15	10	10	10
31	1	1	1	1	1
32	1	1	1	1	2
33	6	4	4	4	4
34	2	2	2	2	2
35	45	28	12	12	10
36	1	1	1	1	1
37	2	2	1	1	1
38	44	31	5	4	4
39	13	7	4	3	3
40	5	3	2	2	2

B. ABLATION EXPERIMENTS

After optimal parameters were determined in our approach, ablation experiments were conducted on the SPSB test database to verify the contribution of the traditional part, network part, and fusion performance. The individual rectification result of each part and the combined result is shown in Table 7, and the corresponding CMC curve is shown in Fig. 24.

The results of the ablation experiment show that each part would contribute to the performance of rectification and combined works best. The traditional part significantly improves the genuine match when the original fingerprint images are of poor quality. The fact indicates the conventional part is robust to interferences commonly appearing in the fingerprints extracted in CSI. The network part improves the genuine match roughly equal regardless of the

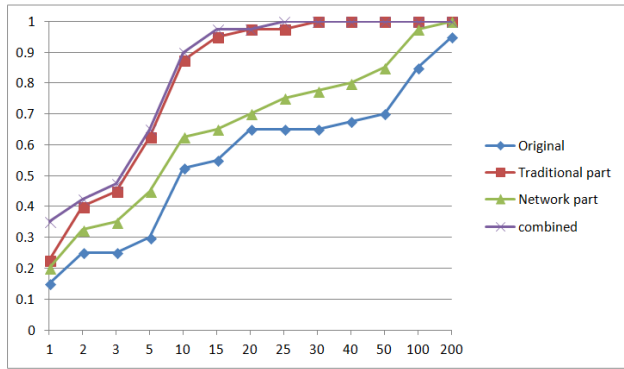


FIGURE 24. The CMC curve of ablation results.

TABLE 7. The compared rank of genuine matches of ablation results.

Number	Original	Traditional part	Network part	combined
1	231	15	65	10
2	4	1	5	1
3	12	1	6	1
4	126	3	7	1
5	18	2	20	1
6	4	4	4	4
7	273	28	151	23
8	59	2	2	1
9	50	10	26	12
10	7	7	1	6
11	1	1	7	1
12	17	4	8	5
13	60	7	35	4
14	16	16	9	13
15	106	12	65	8
16	59	5	51	5
17	2	2	2	2
18	2	2	2	5
19	6	5	6	6
20	1	1	1	1
21	9	1	2	1
22	7	6	6	5
23	39	8	18	7
24	6	7	22	6
25	105	15	43	14
26	1	1	1	1
27	18	4	1	3
28	9	7	15	7
29	54	5	50	6
30	81	9	23	7
31	1	1	1	1
32	2	2	1	1
33	7	4	5	4
34	1	2	1	2
35	88	10	56	7
36	1	1	1	1
37	8	1	3	1
38	108	6	53	1
39	7	3	5	3
40	2	2	2	2

fingerprint image quality. So, the network part could be used to make up for the shortcomings of traditional modules. The coarse-to-fine approach proposed in our paper fuses the advantages of the conventional and network parts. For low-quality fingerprints, our method could strongly resist various interferences compared with the network part. The

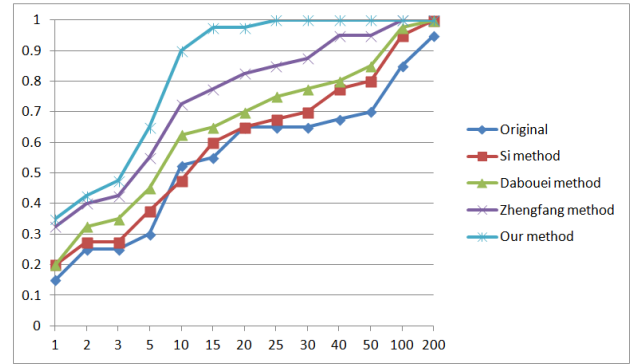


FIGURE 25. The CMC curve of the compared results conducted on the SPSB test database.

TABLE 8. The compared rank of genuine matches conducted on the SPSB test database.

Number	original	Xuanbin	Dabouei	Zhengfang	our
1	231	94	65	40	10
2	4	4	5	2	1
3	12	8	6	8	1
4	126	15	7	6	1
5	18	17	20	13	1
6	4	4	4	4	4
7	273	108	151	74	23
8	59	40	2	1	1
9	50	56	26	18	12
10	7	1	1	1	6
11	1	4	7	1	1
12	17	10	8	8	5
13	60	41	35	1	4
14	16	11	9	5	13
15	106	82	65	33	8
16	59	53	51	3	5
17	2	1	2	1	2
18	2	2	2	1	5
19	6	6	6	6	6
20	1	1	1	1	1
21	9	13	2	4	1
22	7	5	6	2	5
23	39	30	18	12	7
24	6	18	22	4	6
25	105	76	43	25	14
26	1	1	1	1	1
27	18	24	1	10	3
28	9	6	15	9	7
29	54	35	50	29	6
30	81	40	23	17	7
31	1	1	1	1	1
32	2	1	1	1	1
33	7	12	5	6	4
34	1	1	1	1	2
35	88	110	56	90	7
36	1	1	1	1	1
37	8	2	3	2	1
38	108	58	53	37	1
39	7	11	5	5	3
40	2	2	2	1	2

rank of genuine matches improves dramatically, significantly reducing the possibility of missing results. For relatively high-quality fingerprints, our method further improves rectification performance with traditional parts. The rising rank could help experts verify the genuine match faster and more confidently.

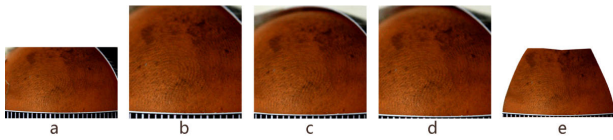


FIGURE 26. Group images of the same fingerprint.

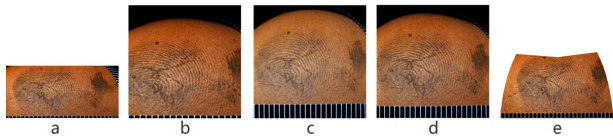


FIGURE 27. Group images of the same fingerprint.

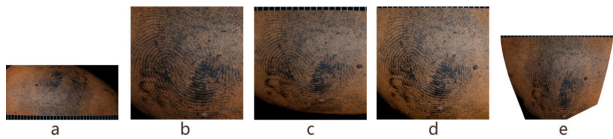


FIGURE 28. Group images of the same fingerprint.

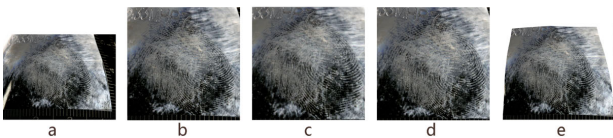


FIGURE 29. Group images of the same fingerprint.

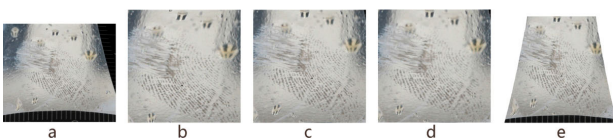


FIGURE 30. Group images of the same fingerprint.

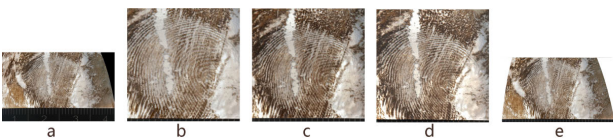


FIGURE 31. Group images of the same fingerprint.

C. COMPARED EXPERIMENTS

We quantitatively evaluated the contribution of the proposed method by conducting experiments on the SPSB test database. Several representative single-image methods were selected as comparison methods.

The ranks of genuine matches are shown in Table 8: original latent fingerprints (no rectification), latent fingerprints rectified by Si et al. approach [13], latent fingerprints rectified by Dabouei et al. approach [24], latent fingerprints rectified by Zhengfang et al. approach [25], and the latent fingerprints rectified by the proposed method. The CMC curve is shown in Fig. 25.

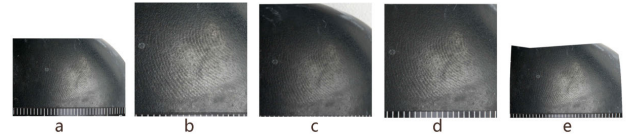


FIGURE 32. Group images of the same fingerprint.

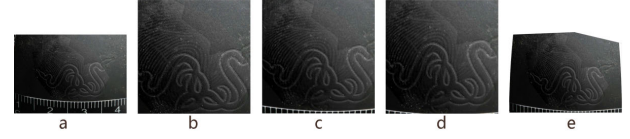


FIGURE 33. Group images of the same fingerprint.

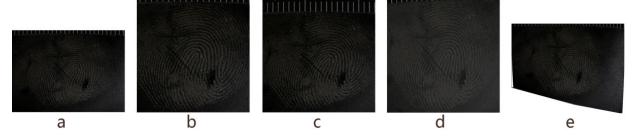


FIGURE 34. Group images of the same fingerprint.

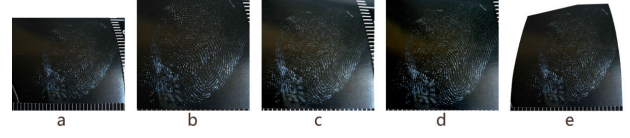


FIGURE 35. Group images of the same fingerprint.

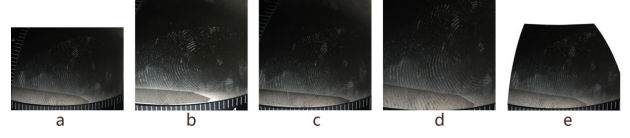


FIGURE 36. Group images of the same fingerprint.



FIGURE 37. Group images of the same fingerprint.

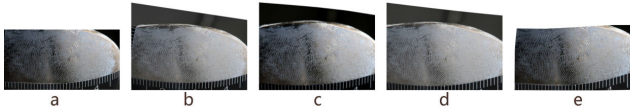


FIGURE 38. Group images of the same fingerprint.

Some visible samples are presented to compare our approach with others in detail. The images from left to right are the (a) original, (b) Xuanbin’s approach, (c) Dabouei’s approach, (d) Zhengfang’s approach, (e) and the proposed approach. The rank of genuine matches is described in the figure note. Such examples are given in Fig. 26-39.

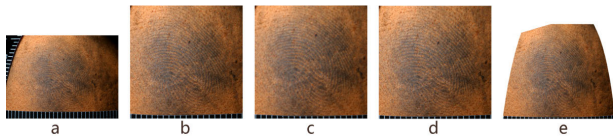


FIGURE 39. Group images of the same fingerprint.

Overlap ridges in the core region are the obstacle to identifying: (a) rank 231, (b) rank 94, (c) rank 65, (d) rank 40, and (e) rank 10.

Attachment to the surface of the object is the obstacle to identify: (a) rank 126, (b) rank 15, (c) rank 7, (d) rank 6, and (e) rank 1.

Severe nonlinear distortion and uneven distribution of magnetic powder are the obstacles to identifying: (a) rank 273, (b) rank 108, (c) rank 151, (d) rank 74, and (e) rank 23.

Excessive 502 glue is the obstacle to identify: (a) rank 60, (b) rank 41, (c) rank 35, (d) rank 1, and (e) rank 4.

Too small a ridge region and a trace of wipe are the obstacles to identify: (a) rank 106, (b) rank 82, (c) rank 65, (d) rank 33, and (e) rank 8.

Blurry ridges in the core region and strip interference are the obstacles to identify: (a) rank 59, (b) rank 53, (c) rank 51, (d) rank 3, and (e) rank 5.

The roughness of the surface of an object is the obstacle to identifying: (a) rank 39, (b) rank 30, (c) rank 18, (d) rank 12, and (e) rank 7.

The interference of the pattern inherent in the object is the obstacle to identifying: (a) rank 6, (b) rank 18, (c) rank 22, (d) rank 4, and (e) rank 6.

Severe nonlinear distortion is the obstacle to identifying: (a) rank 105, (b) rank 76, (c) rank 43, (d) rank 25, and (e) rank 14.

Incoherence and interruption of the ridges are the obstacles to identifying: (a) rank 54, (b) rank 35, (c) rank 50, (d) rank 29, and (e) rank 6.

The missing ridge in the core region is the obstacle to identify: (a) rank 88, (b) rank 110, (c) rank 56, (d) rank 90, and (e) rank 7.

Ridges showing opposite hues in different regions are the obstacle to identifying: (a) rank 108, (b) rank 58, (c) rank 53, (d) rank 37, and (e) rank 1.

See Fig. 26-37 for several examples in which the proposed method is significantly better than the compared approaches. Various factors, such as interference, blur, missing ridges, and severe distortion, can lead to low-quality distorted fingerprints, typical in CSI. The training and testing samples used in the compared methods are far from realistic in forensic practice. The reasons have been explained briefly in Fig. 26-37. Note that the illustration only highlights the primary reason, and the mixture of factors dominates the investigation.

Fig. 38 is an example of equal performance. It is easy for AFIS to match the fingerprint for slight distortion and adequate minutiae. (a) rank 1, (b) rank 1, (c) rank 1, (d) rank 1, and (e) rank 1.

Fig. 39 shows that the performance of the proposed method is not as good as the compared approaches because the image quality is close to the training samples in the compared methods. The ridges are coherent and contrast the background. (a) rank 7, (b) rank 1, (c) rank 1, (d) rank 1, and (e) rank 6.

The results reveal the following. (1) Both rectification algorithms improve the recognition rate compared with the original. (2) Our approach improves matching accuracy in distorted latent fingerprints compared with other approaches [13], [24], [25]. The highest top 25 cumulative match rate of the proposed method is 1, whereas that of the compared methods is not higher than 0.85. (3) The proposed approach significantly achieves improvements compared with the other methods [13], [24], [25] in correcting low-quality distorted fingerprints. For Xuanbin et al.'s approach, rectification performance benefits significantly from detection with the center and upper core points, which are rarely found in CSI. Significant gaps exist in the training and extracted images in CSI for Dabouei et al.'s and Zhengfang et al.'s approaches. As a learning-based method, the similarity between the test and training sets significantly affects performance.

V. CONCLUSION

Fingerprint deformation poses a considerable challenge for fingerprint-matching performance. In CSI, latent fingerprints on curved objects are low-use-rate evidence due to poor image quality and severe distortion. Forensic science cannot adopt most existing rectification methods because (1) a reference fingerprint is a prerequisite for correction, (2) the rectification performance of low-quality fingerprints is poor, and (3) improvements are only verified in small volume databases far from proof in forensic science.

This paper presents a coarse-to-fine algorithm to rectify distorted latent fingerprints. The proposed method combines the advantages of robustness and accuracy when addressing distorted latent fingerprints extracted at crime scenes. The experimental results show that our method improves the matching performance significantly compared with other approaches, especially in low-quality fingerprints.

The limitation of our combined method is that the performance depends on the previous manual processing, including fingerprint extraction and image preprocessing. Future directions could focus on (1) improving accuracy for low-quality fingerprints and (2) reducing reliance on manual operations.

ACKNOWLEDGMENT

(Qing Bao and Ya-Gang Wang contributed equally to this work.)

REFERENCES

- [1] K. Cao, X. Yang, X. Chen, Y. Zang, J. Liang, and J. Tian, "A novel ant colony optimization algorithm for large-distorted fingerprint matching," *Pattern Recognit.*, vol. 45, no. 1, pp. 151–161, Jan. 2012, doi: 10.1016/j.patcog.2011.04.016.
- [2] P. S. Prasad, B. S. Devi, M. J. Reddy, and V. K. Gunjan, "A survey of fingerprint recognition systems and their applications," in *Proc. Int. Conf. Commun. Cyber Physical Eng.* Singapore: Springer, 2019, pp. 513–520, doi: 10.1007/978-981-13-0212-1_53.

- [3] V. N. Dvornychenko and M. D. Garris, "Summary of NIST latent fingerprint testing workshop," Nat. Inst. Standards and Technol., Gaithersburg, MD, USA, Tech. Rep. NIST IR 7377, 2006, doi: [10.6028/NIST.IR.7377](https://doi.org/10.6028/NIST.IR.7377).
- [4] R. Cappelli, D. Maio, D. Maltoni, J. L. Wayman, and A. K. Jain, "Performance evaluation of fingerprint verification systems," *IEEE Trans. Pattern Anal. Mach. Intell.*, vol. 28, no. 1, pp. 3–18, Jan. 2006, doi: [10.1109/TPAMI.2006.20](https://doi.org/10.1109/TPAMI.2006.20).
- [5] D. Maio and D. Maltoni, "Direct gray-scale minutiae detection in fingerprints," *IEEE Trans. Pattern Anal. Mach. Intell.*, vol. 19, no. 1, pp. 27–40, 1997, doi: [10.1109/34.566808](https://doi.org/10.1109/34.566808).
- [6] M. Sabir, T. M. Khan, M. Arshad, and S. Munawar, "Reducing computational complexity in fingerprint matching," *TURKISH J. Electr. Eng. Comput. Sci.*, vol. 28, no. 5, pp. 2538–2551, Sep. 2020, doi: [10.3906/elk-1907-113](https://doi.org/10.3906/elk-1907-113).
- [7] T. J. Jankun-Kelly and K.-L. Ma, "Visualization exploration and encapsulation via a spreadsheet-like interface," *IEEE Trans. Vis. Comput. Graphics*, vol. 7, no. 3, pp. 275–287, Jul./Sep. 2001, doi: [10.1109/2945.942695](https://doi.org/10.1109/2945.942695).
- [8] K. Cao and A. K. Jain, "Automated latent fingerprint recognition," *IEEE Trans. Pattern Anal. Mach. Intell.*, vol. 41, no. 4, pp. 788–800, Apr. 2019, doi: [10.1109/TPAMI.2018.2818162](https://doi.org/10.1109/TPAMI.2018.2818162).
- [9] C. M. Rodriguez, A. de Jongh, and D. Meuwly, "Introducing a semi-automatic method to simulate large numbers of forensic fingermarks for research on fingerprint identification," *J. Forensic Sci.*, vol. 57, no. 2, pp. 334–342, Mar. 2012, doi: [10.1111/j.1556-4029.2011.01950.x](https://doi.org/10.1111/j.1556-4029.2011.01950.x).
- [10] N. Ahmed and A. Varol, "Minutiae based partial fingerprint registration and matching method," in *Proc. 6th Int. Symp. Digit. Forensic Secur. (ISDFS)*, Mar. 2018, pp. 1–5, doi: [10.1109/ISDFS.2018.8355343](https://doi.org/10.1109/ISDFS.2018.8355343).
- [11] X. Chen, J. Tian, and X. Yang, "A new algorithm for distorted fingerprints matching based on normalized fuzzy similarity measure," *IEEE Trans. Image Process.*, vol. 15, no. 3, pp. 767–776, Mar. 2006, doi: [10.1109/TIP.2005.860597](https://doi.org/10.1109/TIP.2005.860597).
- [12] N. K. Ratha, K. Karu, S. Chen, and A. K. Jain, "A real-time matching system for large fingerprint databases," *IEEE Trans. Pattern Anal. Mach. Intell.*, vol. 18, no. 8, pp. 799–813, 1996, doi: [10.1109/34.531800](https://doi.org/10.1109/34.531800).
- [13] X. Si, J. Feng, J. Zhou, and Y. Luo, "Detection and rectification of distorted fingerprints," *IEEE Trans. Pattern Anal. Mach. Intell.*, vol. 37, no. 3, pp. 555–568, Mar. 2015, doi: [10.1109/TPAMI.2014.2345403](https://doi.org/10.1109/TPAMI.2014.2345403).
- [14] D. Wan and J. Zhou, "Fingerprint recognition using model-based density map," *IEEE Trans. Image Process.*, vol. 15, no. 6, pp. 1690–1696, Jun. 2006, doi: [10.1109/TIP.2006.873442](https://doi.org/10.1109/TIP.2006.873442).
- [15] A. Ross, S. C. Dass, and A. K. Jain, "Fingerprint warping using ridge curve correspondences," *IEEE Trans. Pattern Anal. Mach. Intell.*, vol. 28, no. 1, pp. 19–30, Jan. 2006, doi: [10.1109/TPAMI.2006.11](https://doi.org/10.1109/TPAMI.2006.11).
- [16] C. Lin and A. Kumar, "Matching contactless and contact-based conventional fingerprint images for biometrics identification," *IEEE Trans. Image Process.*, vol. 27, no. 4, pp. 2008–2021, Apr. 2018, doi: [10.1109/TIP.2017.2788866](https://doi.org/10.1109/TIP.2017.2788866).
- [17] A. M. Bazen and S. H. Gerze, "Fingerprint matching by thin-plate spline modeling of elastic deformations," *Pattern Recognit.*, vol. 36, no. 8, pp. 1859–1867, 2003, doi: [10.1016/S0031-3203\(03\)00036-0](https://doi.org/10.1016/S0031-3203(03)00036-0).
- [18] J. Feng, Z. Ouyang, and A. Cai, "Fingerprint matching using ridges," *Pattern Recognit.*, vol. 39, no. 11, pp. 2131–2140, Nov. 2006, doi: [10.1016/j.patcog.2006.05.001](https://doi.org/10.1016/j.patcog.2006.05.001).
- [19] S. Gu, J. Feng, J. Lu, and J. Zhou, "Efficient rectification of distorted fingerprints," *IEEE Trans. Inf. Forensics Security*, vol. 13, no. 1, pp. 156–169, Jan. 2018, doi: [10.1109/TIFS.2017.2745685](https://doi.org/10.1109/TIFS.2017.2745685).
- [20] S. Lan, Z. Guo, and J. You, "Pre-registration of translated/distorted fingerprints based on correlation and the orientation field," *Inf. Sci.*, vol. 520, pp. 292–304, May 2020, doi: [10.1016/j.ins.2020.02.017](https://doi.org/10.1016/j.ins.2020.02.017).
- [21] X. Si, J. Feng, B. Yuan, and J. Zhou, "Dense registration of fingerprints," *Pattern Recognit.*, vol. 63, pp. 87–101, Mar. 2017, doi: [10.1016/j.patcog.2016.09.012](https://doi.org/10.1016/j.patcog.2016.09.012).
- [22] S. Lan, Z. Guo, and J. You, "A non-rigid registration method with application to distorted fingerprint matching," *Pattern Recognit.*, vol. 95, pp. 48–57, Nov. 2019, doi: [10.1016/j.patcog.2019.05.021](https://doi.org/10.1016/j.patcog.2019.05.021).
- [23] K. Khongkrapan, "An efficient fingerprint matching by multiple reference points," *J. Inf. Process. Syst.*, vol. 15, no. 1, pp. 22–33, 2019, doi: [10.3745/JIPS.04.0098](https://doi.org/10.3745/JIPS.04.0098).
- [24] A. Dabouei, H. Kazemi, S. M. Iranmanesh, J. Dawson, and N. M. Nasrabadi, "Fingerprint distortion rectification using deep convolutional neural networks," in *Proc. Int. Conf. Biometrics (ICB)*, Feb. 2018, pp. 1–8, doi: [10.1109/ICB2018.2018.00012](https://doi.org/10.1109/ICB2018.2018.00012).
- [25] H. Zhengfang, A. J. P. Delima, I. K. D. Machica, J. C. T. Arroyo, S. Weibin, and X. Gang, "Fingerprint identification based on novel Siamese rectangular convolutional neural networks," *Int. J. Emerg. Technol. Adv. Eng.*, vol. 12, no. 5, pp. 28–37, May 2022, doi: [10.46338/ijetae0522_04](https://doi.org/10.46338/ijetae0522_04).
- [26] X. Guan, Y. Duan, J. Feng, and J. Zhou, "Direct regression of distortion field from a single fingerprint image," in *Proc. IEEE Int. Joint Conf. Biometrics (IJCB)*, Oct. 2022, pp. 1–8, doi: [10.1109/IJCB54206.2022.10007981](https://doi.org/10.1109/IJCB54206.2022.10007981).
- [27] Z. Cui, J. Feng, and J. Zhou, "Dense registration and mosaicking of fingerprints by training an end-to-end network," *IEEE Trans. Inf. Forensics Security*, vol. 16, pp. 627–642, 2021, doi: [10.1109/TIFS.2020.3017926](https://doi.org/10.1109/TIFS.2020.3017926).
- [28] Q. Zheng, X. Tian, M. Yang, Y. Wu, and H. Su, "PAC-Bayesian framework based drop-path method for 2D discriminative convolutional network pruning," *Multidimensional Syst. Signal Process.*, vol. 31, no. 3, pp. 793–827, Jul. 2020, doi: [10.1007/s11045-019-00686-z](https://doi.org/10.1007/s11045-019-00686-z).
- [29] A. Rungchokanun and V. Areekul, "Directionally weighted distance for minutiae-triplets preservation on elastic deformation of fingerprint recognition," *Pattern Recognit. Lett.*, vol. 160, pp. 34–42, Aug. 2022, doi: [10.1016/j.patrec.2022.05.027](https://doi.org/10.1016/j.patrec.2022.05.027).
- [30] C. Dorai, N. K. Ratha, and R. M. Bolle, "Detecting dynamic behavior in compressed fingerprint videos: Distortion," in *Proc. IEEE Conf. Comput. Vis. Pattern Recognit.*, Jun. 2000, pp. 320–326, doi: [10.1109/CVPR.2000.854824](https://doi.org/10.1109/CVPR.2000.854824).
- [31] C. Dorai, N. K. Ratha, and R. M. Bolle, "Dynamic behavior analysis in compressed fingerprint videos," *IEEE Trans. Circuits Syst. Video Technol.*, vol. 14, no. 1, pp. 58–73, Jan. 2004, doi: [10.1109/TCSVT.2003.818354](https://doi.org/10.1109/TCSVT.2003.818354).
- [32] Y. Fujii, "Detection of fingerprint distortion by deformation of elastic film or displacement of transparent board," U.S. Patent 7 660 447, Feb. 9, 2010.
- [33] Y. Zhang, Y. Wu, M. Gao, S. Pan, Z. Shao, and T. Luo, "BlockRFC: Real-time rolled fingerprint construction and distortion rectification," *IEEE Access*, vol. 8, pp. 216948–216959, 2020, doi: [10.1109/ACCESS.2020.3041716](https://doi.org/10.1109/ACCESS.2020.3041716).
- [34] Z. M. Kovacs-Vajna, "A fingerprint verification system based on triangular matching and dynamic time warping," *IEEE Trans. Pattern Anal. Mach. Intell.*, vol. 22, no. 11, pp. 1266–1276, Nov. 2000, doi: [10.1109/34.888711](https://doi.org/10.1109/34.888711).
- [35] K. Anusha and P. V. S. Kumar, "Fingerprint image enhancement for crime detection using deep learning," in *Proc. Int. Conf. Cognitive Intell. Comput.*, 2023, pp. 257–268, doi: [10.1007/978-981-19-2358-6_25](https://doi.org/10.1007/978-981-19-2358-6_25).
- [36] L. Bloy and R. Verma, "Demons registration of high angular resolution diffusion images," in *Proc. IEEE Int. Symp. Biomed. Imaging, From Nano Macro*, Apr. 2010, pp. 1013–1016, doi: [10.1109/ISBI.2010.5490161](https://doi.org/10.1109/ISBI.2010.5490161).
- [37] Z. Tang, P. Xue, P. Yang, D. Jia, and E. Dong, "An effective non-rigid image registration method based on active demons algorithm," in *Proc. IEEE 29th Int. Symp. Comput.-Based Med. Syst. (CBMS)*, Jun. 2016, pp. 124–129, doi: [10.1109/CBMS.2016.18](https://doi.org/10.1109/CBMS.2016.18).
- [38] H. J. Fayad, C. Bakhous, T. Pan, and D. Visvikis, "Optical flow vs bspline image registration for respiratory motion modeling," in *Proc. IEEE Nucl. Sci. Symp. Med. Imag. Conf. Rec. (NSS/MIC)*, Oct. 2012, pp. 3914–3917, doi: [10.1109/NSSMIC.2012.6551898](https://doi.org/10.1109/NSSMIC.2012.6551898).
- [39] D. Karabulut, P. Tertychnyi, H. S. Arslan, C. Ozcinar, K. Nasrollahi, J. Valls, J. Vilaseca, T. B. Moeslund, and G. Anbarjafari, "Cycle-consistent generative adversarial neural networks based low quality fingerprint enhancement," *Multimedia Tools Appl.*, vol. 79, no. 25, pp. 18569–18589, Jul. 2020, doi: [10.1007/s11042-020-08750-8](https://doi.org/10.1007/s11042-020-08750-8).
- [40] Q. Zheng, P. Zhao, Y. Li, H. Wang, and Y. Yang, "Spectrum interference-based two-level data augmentation method in deep learning for automatic modulation classification," *Neural Comput. Appl.*, vol. 33, no. 13, pp. 7723–7745, Jul. 2021, doi: [10.1007/s00521-020-05514-1](https://doi.org/10.1007/s00521-020-05514-1).
- [41] Q. Zheng, P. Zhao, D. Zhang, and H. Wang, "MR-DCAE: Manifold regularization-based deep convolutional autoencoder for unauthorized broadcasting identification," *Int. J. Intell. Syst.*, vol. 36, no. 12, pp. 7204–7238, Dec. 2021, doi: [10.1002/int.22586](https://doi.org/10.1002/int.22586).
- [42] S. Novikov and O. Ushmaev, "Principal deformation of fingerprints," in *Proc. Int. Conf. Audio-Video-Based Biometric Person Authentication*, 2005, pp. 250–259, doi: [10.1007/11527923_26](https://doi.org/10.1007/11527923_26).
- [43] D. Rueckert, A. F. Frangi, and J. A. Schnabel, "Automatic construction of 3-D statistical deformation models of the brain using nonrigid registration," *IEEE Trans. Med. Imag.*, vol. 22, no. 8, pp. 1014–1025, Aug. 2003, doi: [10.1109/TMI.2003.815865](https://doi.org/10.1109/TMI.2003.815865).



QING BAO received the B.E. degree from Shanghai Maritime University, in 2007, and the M.E. degree from the Chinese Criminal Police College, in 2014. He is currently pursuing the Ph.D. degree in control engineering with the University of Shanghai for Science and Technology. His main research interests include pattern recognition and forensic science.



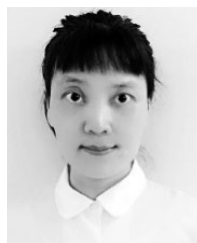
LIANGXIAO SHA received the B.E. degree from the Chinese Criminal Police College, in 2015. His main research interest includes forensic science.



YA-GANG WANG received the B.E. degree in electrical engineering from the China University of Mining and Technology, Beijing, China, in 1988, the M.E. degree in control theory and application from the Taiyuan University of Technology, China, in 1991, and the Ph.D. degree in control theory and control engineering from Shanghai Jiao Tong University, China, in 2000. From 2000 to 2002, he was a Research Fellow with Nanyang Technological University, Singapore. From 2002 to 2007, he was a Senior Engineer with Honeywell (China) Company Ltd. He is currently a Professor with the University of Shanghai for Science and Technology, Shanghai, China. His research interests include process automation, system identification, and wireless sensor networks.



CHANG GAO received the B.E. degree from the Chinese Criminal Police College, in 2015. His main research interest includes forensic science.



FEIFEI LEE (Member, IEEE) received the Ph.D. degree in electronic engineering from Tohoku University, Japan, in 2007. She is currently a Professor with the University of Shanghai for Science and Technology. Her research interests include pattern recognition, video indexing, and image processing.

...